International Journal of Thermal Sciences 49 (2010) 859–866

Contents lists available at ScienceDirect

International Journal of Thermal Sciences

journal homepage: www.elsevier.com/locate/ijts

Experimental investigation of water drop evaporation under moist air or saturated vapour conditions

S. Cioulachtjian [a,*], S. Launay [b], S. Boddaert [c], M. Lallemand [a]

[a] Centre de Thermique de Lyon, UMR 5008, CNRS-INSA-UCB, INSA, 20 Av. Albert Einstein, 69621 Villeurbanne, France
[b] IUSTI, CNRS UMR 6595, Université de Provence, 5 rue Enrico Fermi, 13453 Marseille Cedex 13, France
[c] Centre Scientifique et Technique du Bâtiment, Pôle ENR, Sophia-Antipolis, France

ARTICLE INFO

Article history:
Received 17 March 2009
Received in revised form
24 July 2009
Accepted 24 December 2009
Available online 11 February 2010

Keywords:
Contact angle
Droplet
Evaporation
Silicon
Wettability
Experimental

ABSTRACT

Majority of studies on the drop evaporation phenomena have been realized in air atmosphere environment. Through the present experimental study, we attempt to underline the influence of the gas surrounding the drop during its evaporation in order to give some new physical elements for the modelling of drops or meniscus evaporation. This study has been motivated by the application of two-phase closed systems (heat pipes, loop heat pipes, pulsating heat pipes …), into which liquid and vapour phases are close to the saturation equilibrium state. A silicon wafer substrate, whose roughness does not exceed 3 nm, was selected for the water drop base in order to focus on the gas environment effect on the drop evaporation while reducing the roughness effect. The evaporation of a water drop put on a plane and horizontal silicon surface has been experimentally studied under atmospheric moist air and under saturated vapour conditions at 23 °C. The results show two different behaviours according to surrounding conditions, as well for the contact angle at the equilibrium state, than for the dynamic contact angle during the drop evaporation.

1. Introduction

The capillarity or wettability phenomena play a fundamental role in numerous scientific areas (climate, biological, surface or material sciences, chemistry, etc.), or industrial areas as chemistry (pharmacology, glass industry, automotive, textile, etc.). In general cases, the wettability phenomenon is a consequence of the ability of a liquid to wet a solid structure. The wettability may be characterized by the connecting angle formed between the liquid and the solid wall. Such angle is usually named “wetting contact angle” [1]. In the area of two-phase heat transfers, such as evaporation, boiling or condensation phenomena, the distribution of the liquid and vapour phases may form vapour bubbles, liquid droplets or meniscus on the walls with specific wetting contact angles. According to many authors working on the topics of heat transfer, the region near the interface of the three phases (liquid, vapour and solid wall), also named “triple line”, plays a significant role on the physic of phase change phenomenon [2–4]. As examples, the wettability phenomenon may interact on the wall superheat for bubble nucleation, on the kinetics of the bubble growth or the drop evaporation. The wettability plays also a major role on the thermal–hydraulic operation and the heat transfer performance of two-phase closed systems, such as heat pipes, loop heat pipes, or pulsating heat pipes [5–7]. Thus, in order to predict the heat transfer performance of two-phase closed systems, the contact angle has to be known in either static or dynamic conditions.

Due to the difficulty to determine the liquid/solid surface energy, which would allow calculating the contact angle using Young's equation, the experimental study is the most efficient way to estimate the contact angle in any boundary conditions. Various methods are developed to measure the contact angle. Before introducing these methods, it should be noted that the measurements of the contact angle on real surfaces are always dispersed. Two specific contact angles are then defined: the advancing contact angle θ_a, observed for a liquid/vapour interface passing over a dry surface, and a receding contact angle θ_r, observed for an interface passing over a previously wetted surface. The advancing contact angle is always greater than the receding contact angle. The difference $(\theta_a - \theta_r)$ is called the contact angle hysteresis. In the literature, contact angle hysteresis equal or greater than 10° are mentioned [8–11]. At steady state, the contact angles measured for drops, deposited on a real surface, always range between the two limiting angles θ_a and θ_r. The main causes of the hysteresis and the dispersion of the contact angles are the surface roughness [12], the physical [8,13–15] or chemical surface

* Corresponding author. Fax: +33 472 438 811.
E-mail address: serge.cioulachtjian@insa-lyon.fr (S. Cioulachtjian).

1290-0729/$ – see front matter © 2010 Elsevier Masson SAS. All rights reserved.
doi:10.1016/j.ijthermalsci.2009.12.014

heterogeneities [16], the physical or chemical anisotropies, and the surface deformation. The contact angle and the hysteresis may vary significantly with the drop volume [8,17,18], and/or the fluid adsorption on microporous surfaces [19].

The first method to measure the contact angle is called the sessile drop method. This method, which consists in depositing a liquid drop on a plane and horizontal surface, is the most often used [20,21]. The advancing or receding contact angles are measured by increasing or decreasing the volume of the drop, usually by using a micro-syringe [8]. In the technique suggested by Duncan et al. [22], the tested solid substrate is drilled with a small hole, over which the drop is placed. A micro-syringe, laid under the plate, allows to supply or to evacuate liquid through the hole in order to obtain advancing or receding contact angles, respectively.

The second method, named tilted plate method, consists in laying a drop on a plate, initially horizontal, and then gradually inclined [9,23]. When the plate inclination reaches a critical value, the drop begins to slip (the gravity forces overcome the surface tension forces). Just before the drop slip, the advancing and receding contact angles are located at the front side and at the backside of the drop, respectively. For the small volume drops, the drop slip does not happen systematically, even for inclination close to 90° [24]. For the larger diameter drops, the advancing and receding contact angles strongly depend on the dimensions of the drop, which spreads while sliding on the surface [25].

The third method, the Wilhelmy's method [10,26], consists in moving vertically a thin plate, partially plunged in a liquid bath. The advancing or receding contact angles of the meniscus are obtained by lowering or lifting the plate in the liquid, respectively. This method allows eliminating the drop volume effect on the contact angle value.

Another method to determine the receding contact angle is based on the drop evaporation with or without heating the contact surface (solid wall) [9,27,28]. In the experimental tests of Erbil et al. [9], a water drop is placed on a polymer substrate (PMMA and PET). For a relative humidity of 40% surrounding the drop, Erbil et al. have observed several steps during the drop evaporation. During the first evaporation step, the drop contact angle θ decreases as its base radius R_b remains constant. Then, for a specific value of θ, the drop diameter begins to decrease. Erbil et al. assigned this specific angle to the receding contact angle. Thereafter, the decrease of the drop base radius is going with a succession of regular drop contractions, which induce temporary increases of the contact angle (between 2 and 4°) until the drop disappears. Bourgès-Monnier and Shanahan [29] studied the evaporation effect on the contact angle of a sessile drop of water or n-decane put on insulating material surfaces. The drop and the sample are placed in a closed enclosure initially filled with air saturated with vapour. In the case of a water drop, the use of silica gel into the enclosure tends to reduce the relative humidity, and consequently, induces water evaporation by mass diffusion. In the presence of silica gel and for a water drop on a polished epoxy resin surface, the water evaporation could be decomposed into three steps, for which the contact angle, the height and the base radius of the drop vary distinctly. For the drop evaporation in non-saturated gas and without any wall superheating, the vapour mass diffusion in the gas surrounding the droplet may become the limiting phenomenon on the evaporation kinetic. According to Shahidzadeh-Boun et al. [30], such phenomenon is even more pronounced for the inorganic fluids than for water, caused by the difference of densities between the vapour and the air.

For a drop posed on a heated wall, the interactions between the liquid and the wall play a fundamental role in the evaporation kinetic and in the drop shape evolution. The global evolution of the drop shape (drop base radius, height and contact angle) is usually deduced from the drop visualization with a CCD camera. Thus, the drop behaviours for various couples of liquid/substrate have been analyzed [27,28,31]. During the drop evaporation, two main drop shape evolutions have been observed: 1/constant drop base diameter and 2/constant drop contact angle. As an example, Crafton and Black [32] observed that, for a water drop, the drop base radius remains constant during the evaporation, while, for the heptane drop, the contact angle remains constant. Other global observations on the drop evaporation rate (based on drop volume, weight, or heat flux measurements) indicate a linear increase of the evaporation rate versus the drop base diameter. Analysis of such results lets assume that the evaporation mostly occurs at the triple line.

Through the present experimental study, we attempt to underline the influence of the gas surrounding the drop during its evaporation in order to give some new physical elements for the drop evaporation modelling. This original study has been motivated by the application of two-phase closed systems, into which liquid and vapour phases are closed to the saturation equilibrium state. At the exception of very few studies [33], majority of drop contact angle measurements during evaporation have been realized in atmospheric air environment. The objective of Ponter et al. [33] was to demonstrate that the dependence of contact angle with the drop diameter increases while reducing the fluid saturated pressure in the vessel. As the surface tension is very sensitive to the liquid temperature [34], this study does not allow giving some information on the effect of the gas surrounding on the contact angle and on the drop evaporation.

The question that we attempt to answer in this study is does the gas (atmospheric moist air, or saturated vapour) surrounding the drop plays a significant role on the drop initial contact angle and on the drop shape evolution during evaporation, while keeping constant the vessel temperature? In order to avoid the substrate roughness effect, which may obscure the gas surrounding one, a silicon wafer substrate, whose roughness does not exceed 3 nm, has been selected for the drop base. Another reason to choose such materials is that a silicon substrate may become a material structure of two-phase heat transfer microsystems for electronic cooling, as embedded micro heat pipes [35]. The new measured contact angle could then be useful in the predictive modelling of the thermo-hydraulic behaviours of silicon heat transfer microsystems. It should be noted that, in such gas environment saturated in water vapour, the thermodynamic unbalance for the drop evaporation is induced by a superheating of the wall compared to the fluid saturated state. The effect of the wall superheated on the water drop evaporation has been also investigated.

2. Experimental method

The contact angle of a liquid drop on a heated horizontal plane wall is measured under saturated humid air or pure water-vapour conditions using the experimental set-up shown in Fig. 1a. The cubic enclosure of 60 mm side consists of a double wall into which the water flow is supplied by a thermostated bath to impose a constant and homogenous temperature inside the enclosure. Sight-glass windows close the four lateral faces of the enclosure. The upper face of the enclosure is closed with a silicone disc, into which a micro-syringe goes across in order to put the liquid drop on the sample. The sample support, whose cross-section is shown in Fig. 1b, consists of a brass cylinder of 1.6 mm diameter at its top, laterally isolated with polyvinyl chloride. The thermal contact between the support and the silicon wafer is insured by a thermal bond, whose conductivity is 10 W m^{-1} K^{-1}. A thermocouple, which is inserted inside the brass cylinder, 1 mm under the brass cylinder top surface, allows measuring the wall superheat during the drop evaporation. Immersing the base of the brass cylinder in a heated water tank, whose temperature is controlled, controls the wall superheat.

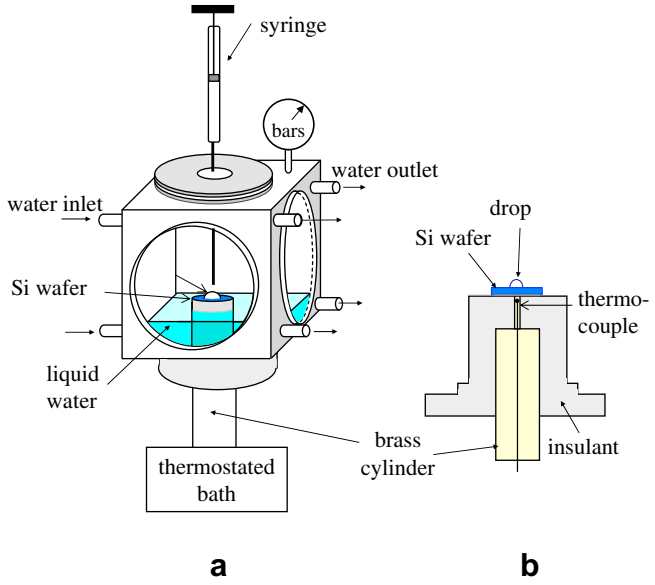

Fig. 1. Test cell – a) general view of the test cell; b) cross-section of the sample support.

The Silicon sample corresponds to a smooth square plate of 6 mm side and 350 μm thick, and has a thermal conductivity of 150 W m^{-1} K^{-1}. According to the high value of the sample thermal conductivity, coupled to the relatively small sample size (the same magnitude order than the drop size) and the low drop evaporation process, a constant and uniform wall temperature may be considered during the drop evaporation time. The silicon wafer surface profile, shown in Fig. 2, has been obtained with an interferometer microscope. The asperity height characterizing the roughness is of the order of few nanometers (Ra = 0.9 nm), i.e. of the order of atomic dimensions. The silicon surface can thus be regarded as completely smooth.

A schematic of the experimental test bench is shown in Fig. 3. A water tank, containing distilled, deionised and degassed water, is connected to the test cell. After being placed under vacuum, the test cell is filled with water until the liquid level is approximately at 3 mm under the sample. A small quantity of this water is pumped with the syringe, initially emptied, before being formed as a droplet on the sample. For each test and before placing the sample into the enclosure, the silicon sample is cleaned of any impurity, by rinsing it with pure acetone, with distilled water and by drying it.

Two series of tests were carried out to study the effect of the gas surroundings on the contact angle of a water drop on silicon wafer at equilibrium state and during evaporation. In both series of tests, the enclosure temperature is maintained at 23 °C, controlled by a water circulation into the double wall of the enclosure. The first series of tests were carried out under saturated moist air atmosphere with a total pressure of 1024 ± 10 mbar (this case is denoted "air" in the figures). The enclosure is closed just after placing the

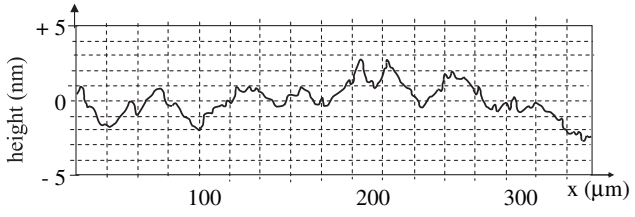

Fig. 2. Roughness profile of a silicon wafer.

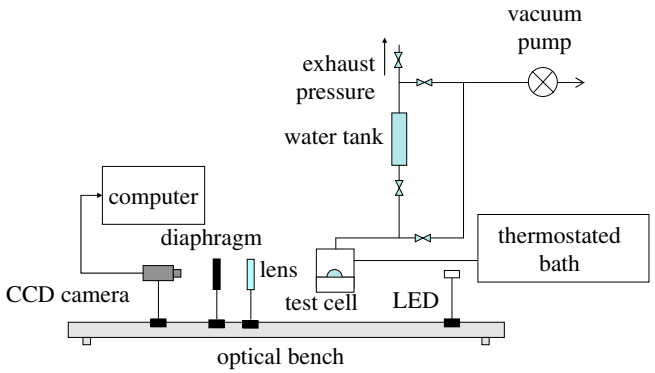

Fig. 3. Experimental set-up.

water drop on the Si sample to avoid any convective effect on the contact angle due to external phenomena. The second series of tests were carried out in saturated vapour conditions, at a pressure of 28 ± 0.5 mbar (this case is denoted "vapour" in the figures). Before filling the enclosure with the degassed water fluid, a primary vacuum until 10^{-3} mbar is achieved. The liquid and vapour temperatures and the pressure inside the enclosure are measured in order to check the saturated equilibrium state.

Once the water drop is placed on the Si wafer, the drop profile shape is thrown on the sensitive cell of a digital camera by lighting the drop using a diffuse white electroluminescent diode. The digital camera with 740 × 940 pixels resolution (Sony DFW700) is connected to a computer and allows the drop image acquisition at different times. The contact angle is directly measured on the photography obtained using a visualization and image processing software. Adjusting the lens position to the camera controls the drop profile magnification. All the components are mounted on an optical bench to allow a precise alignment between the lighting system, the drop, the lens and the camera (Fig. 3). An iris diaphragm has been placed between the lens and the camera in order to check the component alignment, and then, to reduce the geometric aberrations and to optimise the quality of the projected images.

Before each test, the Si wafer is slightly superheated (superheat of about 0.5 K) in order to eliminate eventual micro-drops, which could be formed by condensation on the Si sample surface. It has been observed that such low superheats have no effect on the contact angle of the drop before evaporation. The gas environment in the enclosure is saturated in vapour before and after the drop deposition in order to reduce the drop evaporation during the initial stage, and then, to avoid any surface tension variation due to the drop temperature decreasing. The contact angle is measured approximately 10 s after the syringe is removed, which corresponds to a maximum variation of the drop mass of about 0.2%.

3. Experimental results

3.1. Result analysis

A picture of a water drop placed on a silicon wafer is shown in Fig. 4 for a wall superheat equal to 20 K. Fig. 4a and b represents the drop at the initial state and after a partial evaporation (t = 240 s), respectively. The whole vaporisation duration is equal to 360 s. This drop is axisymmetric and its initial base radius is equal to 1 mm. It has an almost spherical cap form, highlighting the prevalence of capillarity forces on the gravity ones. The gravity effects are negligible for length scale lower than the capillary length L_c, which is equal to 2.7 mm at 23 °C. From the measurements, it can be noted that the water drop keeps a spherical cap form during the major

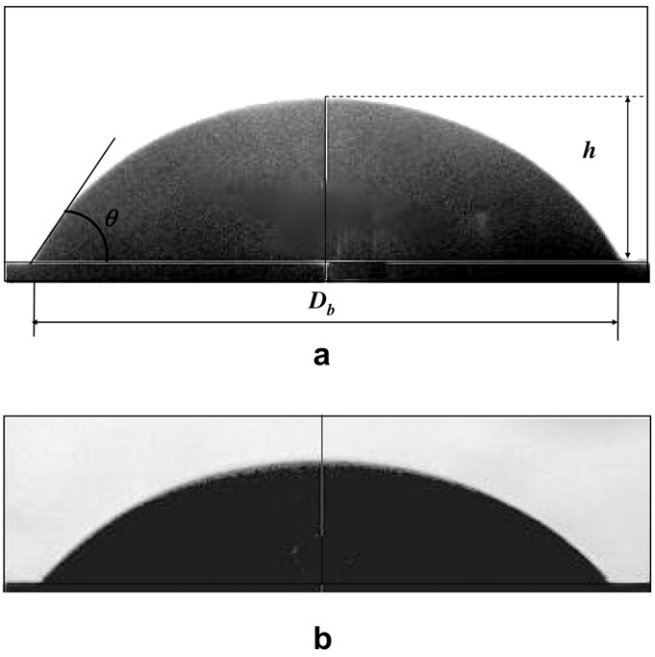

Fig. 4. Photographs of a water drop on a silicon wafer; (a) initial water drop ($R_b = 1$ mm); (b) drop ($R_b = 0.95$ mm) after partial evaporation ($t = 240$ s).

part of the evaporation, whatever the surroundings. A slight flattening of the water drop is observed for drop a base radius higher than 2 mm.

For drops with a spherical cap form, the contact angle θ is deduced from the following equation:

$$h = R_b \tan(\theta/2) \quad (1)$$

The drop volume V and the spherical cap surface area S_c are deduced of the measurements of h and R_b by the following equations:

$$V = \frac{\pi h}{6}\left(h^2 + 3R_b^2\right) \quad (2)$$

$$S_c = \pi\left(h^2 + R_b^2\right) \quad (3)$$

The relative error on h and R_b is about 2%. Using the image processing software, the uncertainty on the θ value does not exceed $\pm 3^\circ$ and the uncertainties on S_c and V are ranged from 4% to 6%. These uncertainties increase as the drop volume decreases because the relative errors on the measurement of h and R_b become larger.

3.2. Influence of the drop surrounding conditions on the initial contact angle θ_i

For the two series of tests, the initial contact angles are compared according to the drop base radius (Fig. 5). The large dispersion of the contact angle measurements may be attributed to the difficulty to repeat identical drop depositions using a syringe. Consequently, the initial contact angle is in between the advancing and receding contact angles. As the test procedure for the drop making at the initial state is similar for the two series of tests (moist air or saturated vapour), the numerous measurement tests allow to preserve a representative value of the initial contact angle in both types of environment. For the tests carried out under atmospheric pressure, the mean value of the contact angle is equal to 78 ± 3°.

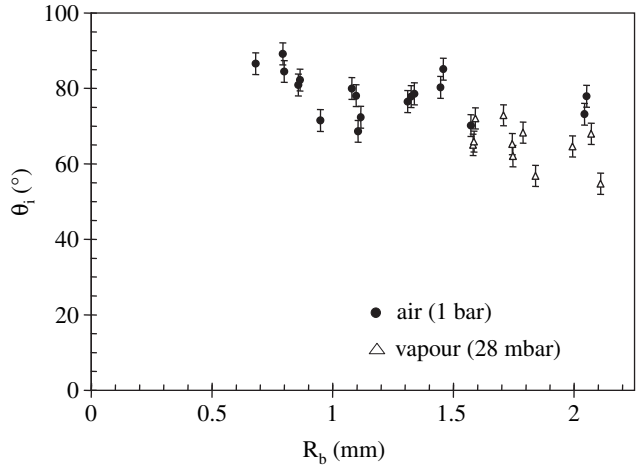

Fig. 5. Dependence of the initial contact angle θ_i on the drop base radius.

The mean value is equal to 64 ± 3° for tests carried out under saturated vapour conditions. The difference between the mean contact angles, which is around 14°, is higher than the measurement uncertainties. Such a difference can be explained neither by the surface roughness, nor by its chemical state. Indeed, similar cleaning processes of the silicon samples have been realized before each series of tests; the silicon wafers are all covered with a nanometric layer of natural oxide. Fig. 6 shows that the difference between the initial contact angles versus the drop volume is the same. For an equivalent drop volume under moist air, the drops have a lower base radius and a higher height, which lead to a larger contact angle, as compared to the drop measured under saturated vapour conditions. As a test, some air was introduced into the enclosure containing the drop under saturated vapour conditions until reaching the atmospheric pressure. Under the effect of the variations of the surroundings conditions, the drop contracted, inducing a decrease of its base diameter and an increase of its height. The increase of the drop contact angle during this test is equal to 6°.

The difference of initial drop contact angles between moist air and vapour environments may be attributed, for one part, to the pressure effect ($P_{air}/P_{vap} = 35$). According to Adamson and Gast [36], an increase of the pressure, while keeping the temperature constant, may tend to increase the surface tension due to the molar

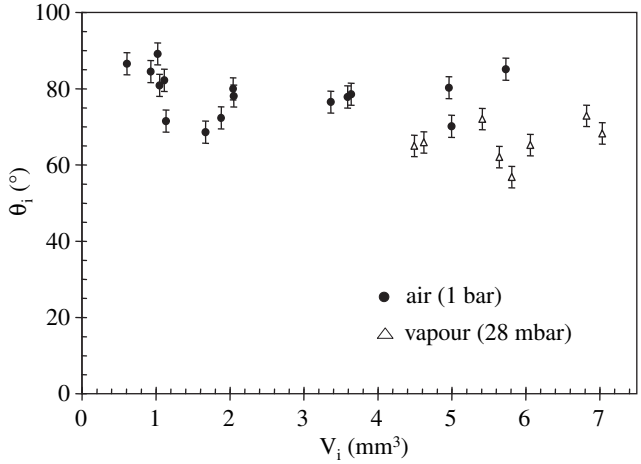

Fig. 6. Dependence of the initial contact angle θ_i on the initial drop volume V_i.

volume change. However, as mentioned by [36], such effect cannot be observed individually as an increase of the pressure at constant temperature is only possible by introducing a second component as an inert gas. Thus, the effect of adsorbed gas at the liquid surface may be associated to the pressure effect on the surface tension variation. The gas or vapour physical adsorption on the substrate wall may also have an effect the wall surface free energy, and consequently, on the drop shape according to the force balance.

3.3. Influence of the gas surrounding conditions on the drop evaporation

According to the present experimental measurements, it has been observed a fundamental role of the gas surrounding conditions during the drop evaporation, and two major effects have been noticed: 1/effect of gas surrounding on the drop shape evolution; 2/effect of gas surrounding on the evaporation rate.

Figs. 7–11 allow comparing the drop shape evolution during evaporation for the two series of tests, for a wall superheat of 20 K. In this study, measurements can be realized until the drop height is equal to 0.1 mm. Beyond this value, the measurement uncertainty becomes too high. Moreover, the drop splits into several small drops before the wall dry-out. The curves of Figs. 7–11 are plotted as function of a normalized time in order to highlight the influence of the gas surrounding on the drop evolution during evaporation. The initial time, when the drop is put on the wall, is noted t_i, and the final time, when the drop has completely disappeared, is noted t_f. The total duration of the drop evaporation is $t_f - t_i$. Then, the normalized time is defined by the ratio:

$$t^* = \frac{t - t_i}{t_f - t_i} \tag{4}$$

The variations of R_b, h and θ under the air surroundings and saturated conditions are presented in Figs. 7 and 8, respectively. For the drop evaporation under moist air (Fig. 7), the drop base radius first remains constant until $t^* < 0.4$, then it decreases progressively until the drop disappears. During the decrease of R_b for t^* ranging from 0.4 to 0.8, θ remains nearly constant at 60°, then it decreases until the end of the evaporation. The drop keeps a spherical cap form during the total drop evaporation time. For the drop evaporation under saturated vapour conditions (Fig. 8), the drop base radius remains constant during the major part of the drop evaporation ($t^* < 0.9$). Consequently, the height and the contact angle of the drop decrease progressively. Near the end of the drop

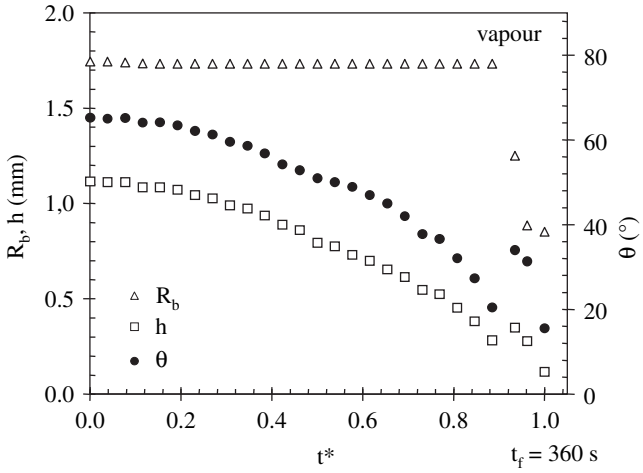

Fig. 8. Variation of R_b, h and θ versus t^* (vapour: 28 mbar, $V_i = 6.1$ mm^3, $\Delta T = 20$ K).

evaporation, for $t^* > 0.9$, a contraction of the drop is observed, which induces a fast decrease of the drop base radius and an increase of the height and the contact angle of the drop.

A normalized contact angle θ^* has been used to make easier the comparison between each test. The normalized contact angle is defined as the ratio between the contact angle at time t and the contact angle at the initial time. The profiles of θ^* during the drop evaporation show clearly the specific evolution depending on the gas surrounding conditions, as moist air or saturated vapour (Fig. 9).

The drop volume V, the solid/liquid interfacial area A_{ls}, and liquid/vapour interfacial area A_{lv}, which are deduced from the measurement of R_b and h, may be interesting to follow as their evolution may help the understandings of the drop evaporation rate. The evolutions of V, A_{ls} and A_{lv} during the drop evaporation are shown in Figs. 10 and 11 for the moist air and saturated vapour conditions, respectively. Under moist air, the contact area A_{ls} is constant at the beginning of the evaporation ($t^* < 0.45$), and then it decreases progressively until the drop disappears. The spherical cap area A_{lv} decreases and tends to A_{ls} at the end of evaporation. Concerning the drop volume, it slowly decreases at the beginning of the evaporation ($t^* < 0.2$) because the drop temperature is initially at the saturation temperature. The drop volume decreases more quickly when the evaporation kinetic increases as the drop

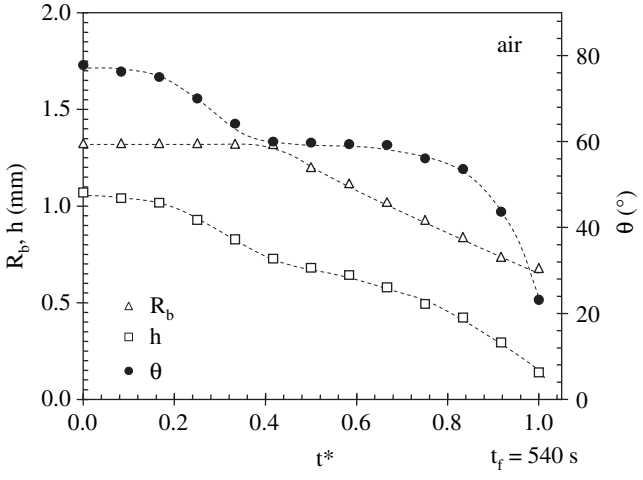

Fig. 7. Variation of R_b, h and θ versus t^* (air: 1 bar, $V_i = 3.6$ mm^3, $\Delta T = 20$ K).

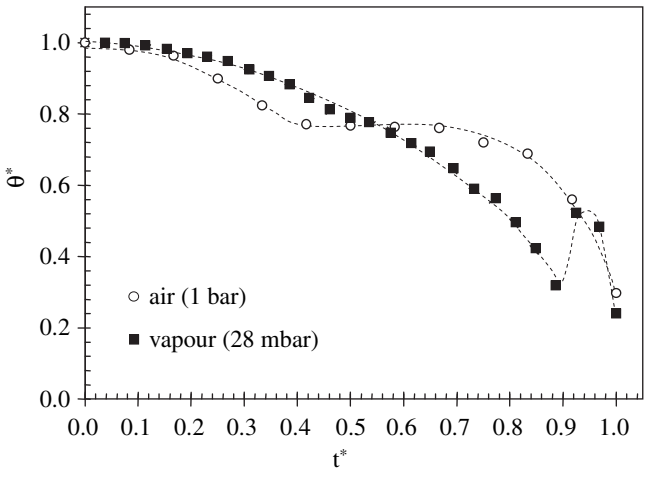

Fig. 9. Variation of θ^* versus t^* ($\Delta T = 20$ K).

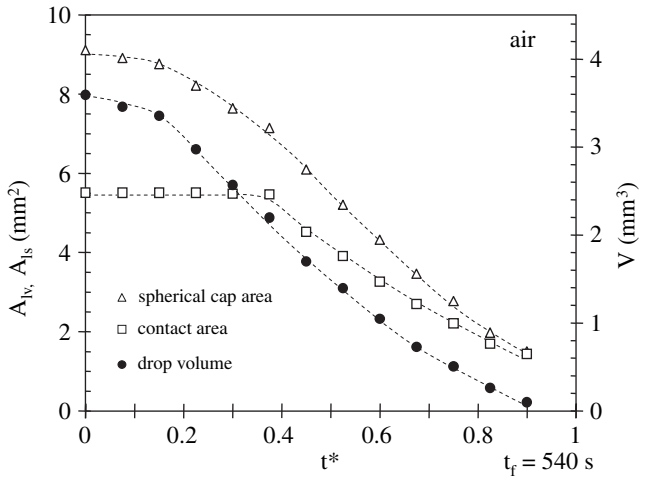

Fig. 10. Variation of liquid/solid and liquid/vapour interfacial areas and drop volume V versus time (air: 1 bar, $V_i = 3.6$ mm^3, $\Delta T = 20$ K).

temperature, heated by the wall, increases. Fig. 11 shows the evolution of the drop geometry during the evaporation under saturated vapour conditions. It differs from those observed during the first series of tests. The drop contact area A_{ls} remains constant until the spherical cap area tends to A_{lv}. At this point, the drop height is very small, and A_{ls} and A_{lv} decrease quickly.

The plots, which are shown in Figs. 7–11, represent the typical trends of the geometrical characteristic evolution of the drop during its evaporation under the two specific gas surroundings (moist air atmosphere and saturated vapour). According to the experimental results, these typical trends are specifics to each gas surroundings, but they seem not depending on the initial drop volume (for drop radius ranged between 0.5 and 2.1 mm).

Following the drop volume parameter for both gas environments, it may be distinguished two specific evolutions, which correspond to two preponderant heat transfer modes.

The first step, for which the drop volume variation is negligible, is defined for t^* ranged in between 0 and 0.2. This step corresponds to the diffusion time of the heat by conduction from the bottom of the brass cylinder, to which a hot temperature is imposed at time 0, to the drop liquid/vapour interface.

The second step, for which t^* is ranged in between 0.2 and 1, is noticed by an almost linear decrease of the drop volume, whatever the initial drop volume and the drop shape evolution occurring during the evaporation process. At this step, the heat, which is transferred through the drop by conduction and convection [37], reaches the liquid/vapour interface. The liquid temperature elevation near the interface induces evaporative cooling heat transfer at the interface. Then, the heat flux transferred from the wall to the vapour may depend on the thermal resistance in the liquid drop and on the vapour diffusion phenomenon from the liquid/vapour interface to the vapour around the drop. As the observations on the drop evaporation indicate a constant evaporation rate whatever the drop shape evolution, the analysis of the present results lets assume that the evaporation rate does not only depend on the geometric factors, as the drop triple line, the liquid/solid or liquid/vapour surface area. In consequence, for the drop evaporation at imposed wall temperature in saturated vapour media, the vapour mass diffusion resistance should be the limited heat transfer.

Fig. 12 allows comparing the typical drop evaporation rate for the two series of tests for a wall superheat of 20 K. It can be noted that the evaporation rate deduced from the measurement is very sensitive to the gas surrounding conditions. Based on numerous tests at $\Delta T = 20$ K, the evaporation rates are equal to 0.007 µl s^{-1} ± 0.002 µl s^{-1} and 0.025 µl s^{-1} ± 0.006 µl s^{-1} for the moist air and saturated vapour surrounding conditions, respectively. The evaporation rate is then 3–4 times faster under saturated vapour pressure than under moist air atmosphere.

The difference of the evaporation rate for drop in moist air atmosphere or in saturated vapour may be attributed to two physical mechanisms. Although the vapour partial pressure should be identical for both gas surrounding conditions, as the enclosure temperature is controlled, the pressure in the liquid phase (drop) is however significantly different. The liquid pressure ratio between the two series of tests, done in air atmosphere or in the saturated vapour conditions, is in the order of magnitude of 35. For the case in air atmosphere, an additional force caused by the air molecules on the liquid/vapour interface conducts the liquid in a subcooled state. Thus, more energy is needed to extract molecules from the liquid drop. Another mechanism, which may explain the reduced evaporation rate in air atmosphere, may be related to the presence of dissolved gas at the liquid/vapour interface. According to Marek and Straub [38], even small contaminations of the surface can significantly reduce the interfacial mass transfer. They concluded that real gas effects should

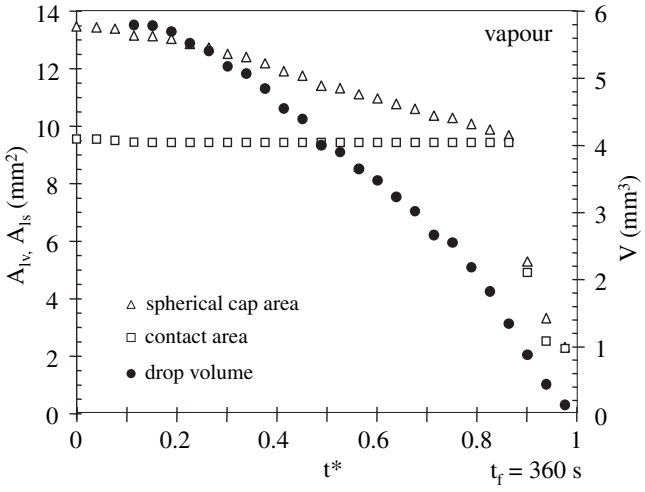

Fig. 11. Variation of liquid/solid and liquid/vapour interfacial areas and drop volume V versus time (vapour: 28 mbar, $V_i = 6.1$ mm^3, $\Delta T = 20$ K).

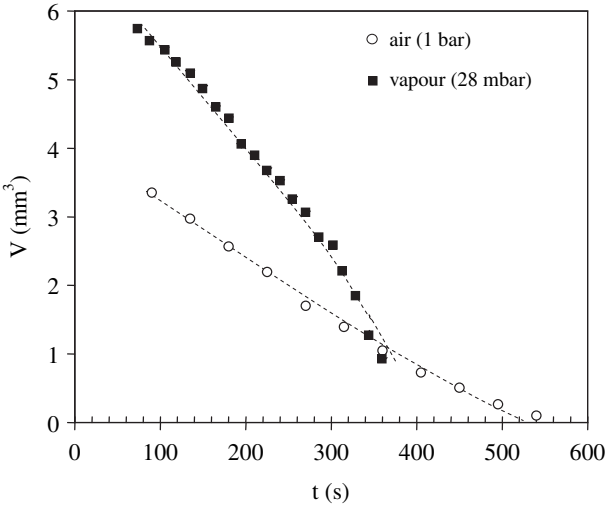

Fig. 12. Variation of θ^* versus t for moist air and vapour conditions ($\Delta T = 20$ K).

be included in the equations of kinetic evaporation to provide better theoretical models for phase change processes.

3.4. Influence of the wall superheat on the contact angle

To highlight the influence of the wall superheat on the contact angle during evaporation, the curves, shown in Figs. 13 and 14, are plotted as functions of a normalized time.

The effect of the wall superheat on the drop contact angle during evaporation under air atmosphere is presented in Fig. 13. The wall superheat ranges from 20 to 37 K. It could be noted that the drop evaporation rate increases with the wall superheat, but the trend of all the curves seems to be not modified by the wall superheat.

Results are different when the tests are carried out under a saturated vapour pressure of 28 mbar. As shown in Fig. 14, the drop evaporation dynamic depends on the wall superheat. During the first seconds of the evaporation ($t^* < 0.3$), no difference on the reduced contact angle has been observed for the different wall superheats. Then, the contact angle varies more quickly for the high wall superheats. When the contact angle θ^* reaches a certain value, varying with the superheat, the drop base radius decreases quickly involving an increase of its contact angle. This minimum corresponding contact angle is called "sliding angle". The contact angle reaches a maximum value smaller than the initial one, and then it decreases again until the drop totally disappears. The same phenomenon is observed for the full range of the wall superheats, but the sliding angle appears faster as the wall superheat increases. Thus, for a wall superheat of 37 K, the sliding corresponds to a reduced time $t^* = 0.6$ with $\theta^* = 0.6$ whereas, for a wall superheat of 20 K, this phenomenon appears for a reduced time $t^* = 0.88$ with $\theta^* = 0.35$. For a wall superheat lower than 20 K, no sliding is observed. Consequently, the sliding angle increases with the wall superheat. The maximum contact angle reached by the drop after sliding also increases with wall superheat. It reaches a value equal to 92% of the initial value for a wall superheat equal to 37 K, but it does not exceed 50% for a wall superheat of 20 K. According to Erbil et al. [9], the sliding angle obtained during the drop evaporation, i.e. the minimal value of θ before its increase, corresponds to the receding angle. These authors obtained many measurements of receding angles, with water drops put on PMMA or PET walls, under atmospheric conditions for a relative humidity equal to 42%. In their tests, the drop water evaporates without external thermal contribution and the time of evaporation is approximately of 2000 s. In the present study, the sliding angles do not appear for tests carried out under atmospheric pressure, but they depend on the wall superheat for tests carried out under saturation conditions.

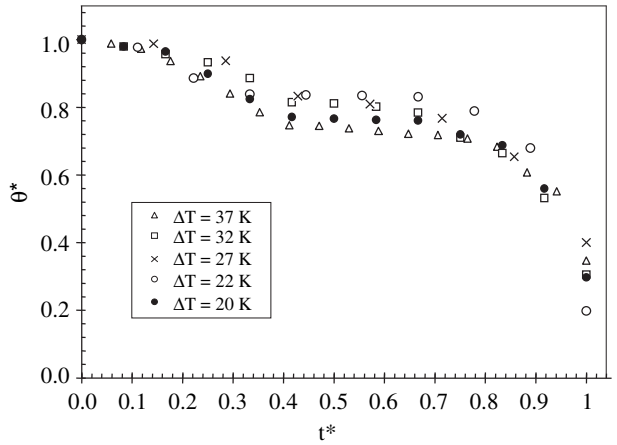

Fig. 13. Variation of θ^* versus t^* for various wall superheats (air: 1 bar).

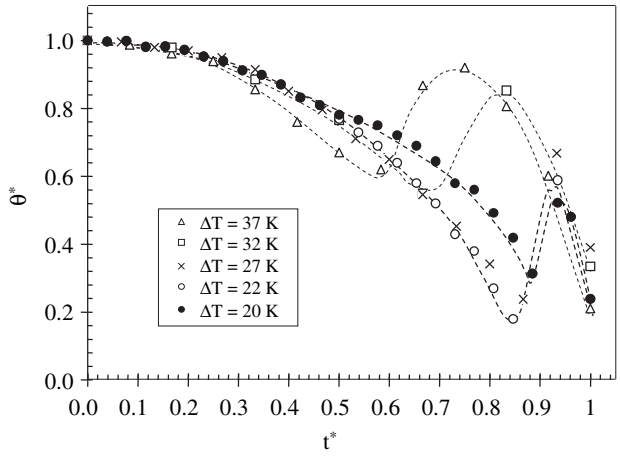

Fig. 14. Variation of θ^* versus t^* for various wall superheats (vapour: 28 mbar).

4. Conclusions

Measurements of drop water contact angle put down on a silicon wafer were carried out under moist air atmospheric pressure (1 bar) and under saturated vapour (28 mbar) at 23 °C. The contact angles were measured at the equilibrium state and during the drop evaporation. The drops of diameter ranging from 1 to 2 mm have a spherical cap form during the drop evaporation under the two conditions. In spite of the very low roughness of the silicon surface, a large dispersion of contact angles was observed.

At the equilibrium state, the mean contact angle is equal to 78° for tests carried out under saturated moist air and equal to 64° for saturated conditions. Such a difference of mean contact angles (14°) is due to the drop surroundings.

For identical drop initial volume and a wall superheat of 20 K, the evaporation rate is 3–4 times faster for the drop under saturated vapour conditions as compared to the drop under saturated moist air.

The drop behaviour during evaporation depends on the surroundings. The drop base radius remains constant during the major part of the evaporation time duration under saturated conditions, whereas there exists several steps for which the drop base radius and the contact angle may decrease independently under air atmosphere.

At the difference of tests carried out under air atmosphere, the drop evaporation behaviour under saturated conditions is dependent of the wall superheat.

These results highlight the importance of the surroundings on the dynamics of drop evaporation. In consequence, under conditions of saturation, it is not convenient to use values of contact angle obtained from tests carried out under air atmosphere conditions.

References

[1] P.-G. de Gennes, F. Brochard-Wyart, D. Quéré, Capillarity and Wetting Phenomena: Drops, Bubbles, Pearls, Waves. Springer ed., 2002.
[2] V.P. Carey, Liquid-Vapor Phase-Change Phenomena: An Introduction to the Thermophysics of Vaporization and Condensation Processes in Heat Transfer Equipment. Taylor & Francis, 1992.
[3] A. Faghri, Heat Pipe Science and Technology. Taylor & Francis, New York, 1995.
[4] P. Stephan, J. Kern, Evaluation of heat and mass transfer phenomena in nucleate boiling. Int. J. Heat Fluid Flow 25 (2) (2004) 140–148.
[5] S. Launay, V. Sartre, M.B.H. Mantelli, K. Vieira de Paiva, M. Lallemand, Investigation of a wire plate micro heat pipe array. Int. J. Thermal Sci. 43 (5) (2004) 499–507.
[6] S. Launay, V. Sartre, J. Bonjour, Parametric analysis of loop heat pipe operation: a literature review. Int. J. Thermal Sci. 46 (7) (2007) 621–636.
[7] S. Khandekar, M. Groll, P. Charoensawan, P. Terdtoon, Pulsating heat pipes: thermo-fluidic characteristics and comparative study with single phase

thermosyphon, in: Proceedings of 12th International Heat Transfer Conference, Grenoble, France, vol. 4, 2002, pp. 459–464.
[8] J. Drelich, J.D. Miller, R.J. Good, The effect of drop (bubble) size on advancing and receding contact angles for heterogeneous and rough solid surfaces as observed with sessile-drop and captive-bubble techniques. J. Colloid Interface Sci. 179 (1996) 37–50.
[9] H.Y. Erbil, G. McHale, S.M. Rowan, M.I. Newton, Determination of the receding contact angle of sessile drops on polymer surfaces by evaporation. Langmuir 15 (1999) 7378–7385.
[10] K. Abe, H. Takiguchi, K. Tamada, Dynamic contact angle measurement of Au (111)-thiol self-assembled monolayers by the Wilhelmy plate method. Langmuir 16 (2000) 2394–2397.
[11] C.N.C. Lam, N. Kim, D. Hui, D.Y. Kwok, M.L. Hair, A.W. Neumann, The effect of liquid properties to contact angle hysteresis. Colloids Surf. A Physicochem. Eng. Aspect 189 (2001) 265–278.
[12] F.Y.H. Lin, D. Li, A.W. Neumann, Effect of surface roughness on the dependence of contact angles on drop size. J. Colloid Interface Sci. 159 (1993) 86–95.
[13] J. Drelich, J.D. Miller, The effect of solid surface heterogeneity and roughness on the contact angle/drop (bubble) size relationship. J. Colloid Interface Sci. 164 (1994) 252–259.
[14] A. Marmur, Contact angle hysteresis on heterogeneous smooth surfaces. J. Colloid Interface Sci. 168 (1994) 40–46.
[15] F.Y.H. Lin, D. Li, The effect of surface heterogeneity on the drop size dependence of contact angles. Chem. Eng. Sci. 50 (1995) 2633–2639.
[16] J.N. Israelachvili, M.L. Gee, Contact angles on chemically heterogeneous surfaces. Langmuir (1989) 288–289.
[17] W.J. Herzberg, J.E. Marian, Relationship between contact angle and drop size. J. Colloid Interface Sci. 33 (1970) 161–163.
[18] Y. Gu, Drop size dependence of contact angles of oil drops on a solid surface in water. Colloids Surf. A Physicochem. Eng. Aspect 181 (2001) 215–224.
[19] R.V. Sedev, J.G. Petrov, A.W. Neumann, Effect of swelling of a polymer surface on advancing and receding contact angles. J. Colloid Interface Sci. 180 (1996) 36–42.
[20] A.W. Neumann, R.J. Good, in: R.J. Good, R.R. Stromberg (Eds.), Surface and Colloid Sciences, Experimental Methods, vol. 11, Plenum Press, New York, 1979, pp. 31–91.
[21] H.Y. Erbil, R.A. Meric, Evaporation of sessile drops on polymer surfaces: ellipsoidal cap geometry. J. Phys. Chem. B 101 (1997) 6867–6873.
[22] D. Duncan, D. Li, J. Gaydos, A.W. Neumann, Correlation of line tension and solid–liquid interfacial tension from the measurement of drop size dependence of contact angles. J. Colloid Interface Sci. 169 (2) (1995) 256–261.
[23] C.W. Extrand, Y. Kumagai, An experimental study of contact angle hysteresis. J. Colloid Interface Sci. 191 (1997) 378–383.
[24] S. Cioulachtjian, S. Launay, M. Lallemand, Angles de contact en milieu saturé d'une goutte d'eau sur une surface d'oxyde de silicium. Congrès Français de Thermique, SFT 2000. Elsevier, 2000, pp. 403–407.
[25] C.W. Extrand, Y. Kumagai, Liquid drops on an inclined plane: the relation between contact angles, drop shape, and retentive force. J. Colloid Interface Sci. 170 (1995) 515–521.
[26] H. Kamusewitz, W. Possart, D. Paul, The relation between Young's equilibrium contact angle and the hysteresis on rough paraffin wax surfaces. Colloids Surf. A 156 (1999) 271–279.
[27] J.D. Bernardin, I. Mudawar, C.B. Walsh, E.I. Franses, Contact angle temperature dependence for water droplets on practical aluminum surfaces. Int. J. Heat Mass Transfer 40 (5) (1997) 1017–1033.
[28] L. Grandas, C. Reynard, R. Santini, L. Tadrist, Etude expérimentale de l'évaporation d'une goutte posée sur une plaque chauffante. Influence de la mouillabilité. Int. J. Thermal Sci. 44 (2005) 137–146.
[29] C. Bourgès-Monnier, M.E.R. Shanahan, Influence of evaporation on contact angle. Langmuir 11 (1995) 2820–2829.
[30] N. Shahidzadeh-Bonn, S. Rafaï, A. Azouni, D. Bonn, Evaporating droplets. J. Fluid Mechanics 549 (2006) 307–313.
[31] S. David, K. Sefiane, L. Tadrist, Experimental investigation of the effect of thermal properties of the substrate in the wetting and evaporation of sessile drops. Colloids Surf. A Physicochem. Eng. Aspect 298 (1–2) (2007) 108–114.
[32] E.F. Crafton, W.Z. Black, Heat transfer and evaporation rates of small liquids droplets on heated horizontal surfaces. Int. J. Heat Mass Transfer 47 (2004) 1187–1200.
[33] A.B. Ponter, A.P. Boyes, The relation between contact angle and drop size for water at its boiling point for a pressure range 50–760 Torr. Can. J. Chem. 50 (15) (1972) 2419–2422.
[34] Neil Kensington Adam, The Physics and Chemistry of Surfaces, third ed. Oxford University Press, 1941, 436 pp.
[35] S. Launay, V. Sartre, M. Lallemand, Experimental study on silicon micro-heat pipe arrays. Appl. Thermal Eng. 24 (2–3) (2004) 233–243.
[36] A.V. Adamson, A.P. Gast, Physical Chemistry of Surfaces, sixth ed. John Wiley & Sons, 1997, 784 p.
[37] D. Bonn, J. Eggers, J. Indekeu, J. Meunier, E. Rolley, Wetting and spreading. Rev. Modern Phys. 81 (2009) 739–805.
[38] R. Marek, J. Straub, Analysis of the evaporation coefficient and the condensation coefficient of water. Int. J. Heat Mass Transfer 44 (2001) 39–53.